Eur. Phys. J. C 34, 173–180 (2004)
Digital Object Identifier (DOI) 10.1140/epjc/s2004-01672-1

THE EUROPEAN PHYSICAL JOURNAL C

Cross sections for multi-particle final states at a linear collider

T. Gleisberg[1a], F. Krauss[1,2b], C.G. Papadopoulos[2,3c], A. Schälicke[1d], S. Schumann[1e]

[1] Institut für Theoretische Physik, TU Dresden, 01062 Dresden, Germany
[2] Theory Division, CERN, 1211 Geneva 23, Switzerland
[3] Institute of Nuclear Physics, NCSR Demokritos, 15310 Athens, Greece

Received: 26 November 2003 / Revised version: 15 January 2004 /
Published online: 3 March 2004 –

Abstract. In this paper total cross sections for signals and backgrounds of top- and Higgs-production channels in e^+e^- collisions at a future linear collider are presented. All channels considered are characterized by the emergence of six-particle final states. The calculation takes into account the full set of tree-level amplitudes in each process. Two multi-purpose parton level generators, HELAC/PHEGAS and AMEGIC++, are used, and their results are found to be in perfect agreement.

1 Introduction

Six-particle final states constitute the signature for many processes that will be studied at the precision level at a future e^+e^- linear collider. Important channels include the production and decay of top quark pairs and – if existent – of one or more Higgs bosons, the latter process allowing a test to be made of the structure of the Higgs potential. Furthermore, if no evidence for a Higgs boson was found at the LHC, the study of quartic gauge boson couplings is mandatory in order to understand alternative scenarios of electroweak symmetry breaking. Leaving the framework of the standard model (SM) the production of, say, chargino pairs in the minimal supersymmetric standard model (MSSM) will lead to six-particle final states as well. To understand these processes at the precision level, i.e. at the order of a few per cent, it is mandatory to supplement typical approaches such as the narrow-width approximation, with corresponding calculations through full amplitudes, and to quantify the effect of non-resonant contributions. Obviously, for hadronic final states, a full QCD calculation is unavoidable.

Such investigations, however, are a formidable calculational task that cannot be handled without dedicated computer programs. Two major difficulties make these necessary.
(1) Including the full SM for the production of a six-particle final state often leads to having to handle a large number of diagrams. As an illustrative example of this problem, take the process $e^+e^- \to e^+e^-e^+e^-e^+e^-$, which results in 13896 Feynman diagrams. Obviously, the common textbook method of squaring the diagrams, by employing completeness relations for the external particles and evaluating the traces, is not a very efficient way to calculate the matrix element squared.
(2) Apart from the treatment of an enormous number of diagrams, growing roughly factorially with the number of external legs, the integration over the phase space of the outgoing particles becomes a tedious task. The high dimensionality, $3n-4$, for n final-state particles necessitates the use of Monte Carlo methods. To achieve convergence of the Monte Carlo procedure process- and cut-dependent phase-space mappings are required that tame wildly fluctuating integrands, which are due to nearly on-shell propagators. A benefit of Monte Carlo methods, if carefully implemented, is that not only total cross sections but also distributions including all possible types of kinematical cuts can be calculated on an equal footing.

In the past years, different types of parton level generators have been constructed. They can be crudely characterized as either specialized or multi-purpose generators.

Usually, the former ones contain explicit matrix elements and phase-space mappings for specific classes of processes with specific assumptions. These matrix elements were constructed before outside the respective program, and this feature also allows for instance to implement non-universal higher order corrections in a controlled way. Often, the phase-space mappings can be optimized before as well.

Examples for such programs dealing with some of the processes discussed here are LUSIFER [4] and eett6f [5]. LUSIFER provides all six-fermion final states, including QCD contributions for up to four final-state quarks. External fermions within LUSIFER are assumed to be massless. The program eett6f is specialized in top quark pair

[a] e-mail: tanju@theory.phy.tu-dresden.de
[b] e-mail: Frank.Krauss@cern.ch
[c] e-mail: Costas.Papadopoulos@cern.ch
[d] e-mail: dreas@theory.phy.tu-dresden.de
[e] e-mail: steffen@theory.phy.tu-dresden.de

production channels, here the outgoing fermions might be massive. Both programs use versions of the adaptive multichannel method in the spirit of [6] for their integration. A further dedicated program using the multichannel importance sampling is SIXFAP [7]. It provides the electroweak contributions for a large set of six-fermion final states, taking into account possible non-zero fermion masses.

In contrast to specialized programs, multipurpose codes generate both the matrix elements and the phase-space mappings with or without some intervention by the user. Apart from the programs used in this paper, examples of these types of programs are O'Mega/Whizard [8, 9] and MadGraph/MadEvent [10, 11]. In the first package, O'Mega [8] relies on a version of the alpha algorithm [12]. However, in the present version of O'Mega, full QCD has not been implemented yet. The integration of the resulting matrix elements is achieved through Whizard [9], which constructs phase-space mappings automatically and integrates them with the VAMP algorithm [13]. In fact, Whizard can also be interfaced with other matrix element generators and it can be used to generate unweighted, single events. In contrast, MadGraph/MadEvent generates all Feynman diagrams for a process under consideration and then passes the information to the HELAS package [14] for the translation into corresponding helicity amplitudes. The integration channels are constructed automatically, and a new version of the adaptive multichannel method described in [11] is employed for the actual integration and the generation of unweighted events.

This paper deals with the calculation of total cross sections for many relevant processes at a future e^+e^- collider with two different, independent packages, namely HELAC/PHEGAS and AMEGIC++. Similar to the comparison of four-fermion generators at the LEP2 Monte Carlo Workshop [15], a detailed study and mutual benchmarking of tools for six- and eight-particle final states at a future linear collider has been initiated in the framework of the extended ECFA/DESY study [16]. Here, a further step into this direction is reported.

For the case of exclusively massless final-state particles, an extended comparison for a large set of six-fermion final states between the programs LUSIFER and MADGRAPH has been presented in [4]. The phase-space integration for the latter program has been done by WHIZARD. Beside the comparison of total cross sections relevant for a 500 GeV collider the authors present some phenomenologically relevant differential distributions for off-shell top quark pair production and Higgs boson production in the intermediate Higgs mass range. In addition the influence of initial-state radiation has been investigated. The two programs to be studied within this work have been cross checked for a large set of processes against the results presented in [4]. For all channels considered an agreement within two to three standard deviations has been achieved. In addition, a compendium of results achieved by different generators, including HELAC/PHEGAS and AMEGIC++, for selected top quark pair production channels in the massless fermion approximation can be found in [17].

This paper is organized as follows. In Sect. 2 and 3 the relevant features of the two programs, HELAC/PHEGAS and AMEGIC++, are briefly reviewed. In Sect. 4 the results are presented and discussed. Conclusions are drawn in Sect. 5.

2 The HELAC/PHEGAS package

2.1 Amplitude computation: HELAC

The traditional representation of the scattering amplitude in terms of Feynman graphs results in a computational cost that grows like the number of those graphs, therefore as $n!$, where n is the number of particles involved in the scattering process.

An alternative to the Feynman graph representation is provided by the Dyson–Schwinger approach.

Dyson–Schwinger equations recursively express the n-point Green functions in terms of the 1-,2-,..., $(n-1)$-point functions. For instance in QED these equations can be written as follows:

(1)

$$b^\mu(P) = \sum_{i=1}^{n} \delta_{P=p_i} b^\mu(p_i) + \sum_{P=P_1+P_2} (\mathrm{i}g) \Pi^\mu_\nu \, \bar\psi(P_2)\gamma^\nu\psi(P_1)\epsilon(P_1,P_2), \tag{2}$$

where

$b_\mu(P)$ =  $\psi(P)$ =  $\bar\psi(P)$ =  (3)

describes a generic n-point Green function with one outgoing photon, fermion or antifermion leg, respectively, carrying momentum P. $\Pi_{\mu\nu}$ stands for the boson propagator and ϵ takes into account the sign due to fermion antisymmetrization.

Technical details about the implementation of the algorithm for the electroweak interactions can be found in [1].

For QCD amplitudes, color representation and summation play an important role. Usually, for the n-gluon amplitude the well-known color decomposition is used:

$$\mathcal{M} = 2\mathrm{i}g^{n-2} \sum_{P(2,\ldots,n)} \mathrm{Tr}(t^{a_1}\ldots t^{a_n}) \mathcal{C}(1,\ldots,n). \tag{4}$$

For processes involving quarks a similar expression may be derived. For further details, the reader is referred to the vast literature on the subject [18]. Methods for calculating the C-functions have been developed [19], including some recent ones, more suitable for multiparticle processes [20, 21]. One of the most interesting aspects of this

decomposition is the fact that the C-functions satisfy certain useful properties, such as gauge invariance and cyclic symmetry. Nevertheless, the computational complexity is rather high and the evaluation of the squared color matrix a rather complicated task [22].

In HELAC a novel approach has been considered. It is based on the color connection (or color flow) representation of the interaction vertices, where the explicit reference to the color has been avoided, as is also the case in the usual color decomposition. The advantage, however, is that the color factors acquire a much simpler form, which moreover holds for gluon as well as for quark amplitudes, leading to a unified approach *for any tree-order process involving any number of colored partons*. Moreover, the unweighting procedure is significantly facilitated, since the usual information on color connections, needed by the parton shower Monte Carlo, is automatically available, without any further calculation. The color factor is universally given by

$$\mathcal{F}_I = \delta_{1\sigma_I(1)}\delta_{2\sigma_I(2)}\dots\delta_{n\sigma_I(n)}\,, \tag{5}$$

whereas the color matrix, defined as

$$\mathcal{M}_{IJ} = \sum_{\text{colors}} \mathcal{F}_I\mathcal{F}_J^\dagger, \tag{6}$$

with the summation running over all colors, $1,\dots,N_c$, has a very simple representation:

$$\mathcal{M}_{IJ} = N_c^{m(\sigma_I,\sigma_J)}\,. \tag{7}$$

Here, $1 \le m(\sigma_I,\sigma_J) \le n$ counts the number of cycles made by the elements of the permutations σ_I and σ_J. Details can be found in [23].

2.2 Phase-space integration: PHEGAS

The study of multiparticle processes, such as six-fermion production in e^+e^-, requires efficient phase-space Monte Carlo generators. The reason is that the squared amplitude, being a complicated function of the kinematical variables, exhibits strong variations in specific regions and/or directions of the phase space, lowering in a substantial way the speed and the efficiency of the Monte Carlo integration. A well-known way out of this problem relies on algorithms characterized by two main ingredients:
(1) the construction of appropriate mappings of the phase-space parametrization, in such a way that the main variation of the integrand can be described by a set of almost uncorrelated variables, and
(2) a self-adaptation procedure that reshapes the generated phase-space density in order to be as close as possible to the integrand.

In order to construct appropriate mappings, it is important to note that the integrand, i.e. the squared amplitude, has a well-defined representation in terms of Feynman diagrams. It is therefore natural to associate to each Feynman diagram a phase-space mapping that parametrizes the leading variation coming from it. In PHEGAS, information from HELAC is used to automatically construct a representation of all Feynman graphs contributing to the given process. The subset of Feynman graphs that results in a different phase-space parametrization is then used as kinematical mappings, called channels, to perform the Monte Carlo integration. Details can be found in [2].

Since in six- and eight-fermion production a large number of kinematical channels contribute, typically of the order of 10^2 to 10^4, the optimization is also used to reduce their number. This is based on the fact that many of the channels exhibit an important correlation that renders them practically useless as separate channels. The reduction in the number of channels achieved by this optimization is generally important, resulting in a very efficient and rapid integration.

The main points can be summarized as follows.
(1) The algorithm exhibits a computational cost that grows like $\sim 3^n$, in contrast to the $n!$ growth of the Feynman graph approach. Therefore there is no severe limitation in computing many-particle amplitudes and the computation of processes involving 10 or more external particles is within reach [24].
(2) All electroweak vertices in both the Feynman and the Unitary gauge have been included, allowing highly non-trivial checks to be performed. The QCD interactions have been implemented in the color connection representation, allowing also a fast unweighting procedure to be followed. The decay width of unstable particles [25] is introduced in the fixed-width and complex-mass schemes [26]. Any process with any type of standard model particle can be reliably computed.
(3) Special features include also the possibility to use higher precision floating point arithmetic, allowing full control over all possible phase-space regions. Speeding up techniques, for helicity the Monte Carlo treatment and large N_c estimates, are also available.
(4) Incorporation of higher order corrections, besides initial state radiation (currently available fermion-loop corrections up to three-point functions), and the implementation of the four-point function fermion-loop corrections and of the minimal supersymmetric standard model are in progress.

3 The program AMEGIC++

AMEGIC++, acronym for (A Matrix Element Generator In C++), is a multi-purpose parton level generator written in C++. It provides a convenient tool for the calculation of cross sections for scattering processes at the tree level in the framework of the SM and the MSSM, allowing for the inclusion of initial state radiation through the structure function approach. Recently the code was extended to cover processes in the ADD model of large extra dimensions as well [27]. The program can also be used to generate single events and it is one of the modules for the new complete event simulation framework SHERPA [28]. As such, the single events of AMEGIC++ can be handed over to the parton shower module APACIC++ [29] with the help of a new method that is correct at the next-to-leading

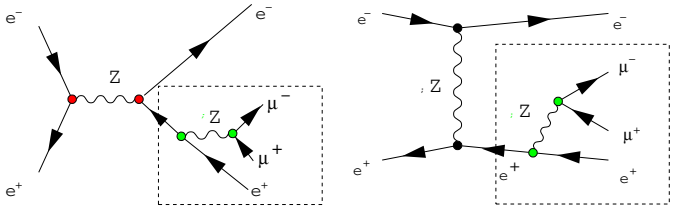

Fig. 1. Factoring out common pieces of amplitudes with identical color structure. In the example above, the parts within the boxes are identical; hence the two amplitudes can be added, and the terms inside the box can be factored out

logarithmic accuracy [30] and are thus linked correctly to fragmentation.

In AMEGIC++, full sets of Feynman diagrams are constructed automatically and are translated by the program into helicity amplitudes in a formalism similar to the one in [31]. The color structure of each diagram is represented as a word string, the emerging structures are grouped into sets of amplitudes with identical, common color structure. Based on them, a matrix of color factors between amplitudes is calculated using the ordinary $SU(3)$ algebra. A number of refinements of the helicity method has been implemented within the code as well. First of all, the algorithm presented in [32] fixes the relative signs of amplitudes when Majorana fermions are present. Furthermore, explicit polarizations for massive or massless external spin-1 bosons are enabled, allowing us to consider polarized cross sections. Similar considerations help to replace numerators of spin-1 propagators by summing over suitably defined polarizations for off-shell particles disentangling nested Lorentz structures emerging for amplitudes with many internal spin-1 bosons. As a result, AMEGIC++ needs only quite a limited set of building blocks to construct all helicity amplitudes. Internally, they are represented as word strings employing some knowledge-storing mechanism that ensures that all building blocks have to be evaluated only once for each call of the full matrix element. With the help of internal methods these word strings are further simplified. Furthermore, another massive gain in efficiency has been achieved by summing amplitudes with identical color structure and by algorithms for finding common factors. This is exemplified in Fig. 1. Having performed these manipulations, the resulting helicity amplitudes are stored in library files.

The introduction of finite-width effects while maintaining $U(1)$ and $SU(2)$ gauge invariance has been subject of many studies [25]. Within AMEGIC++ the fixed-width scheme (FWS) and the gauge invariance preserving complex-mass scheme (CMS) [26] are supported. The effects of gauge invariance violation in the FWS turned out to be strongly suppressed [4,26], leaving this simple scheme still useful for practical calculations.

Defining the complex-mass parameters of the electroweak gauge bosons, the Higgs boson and the top quark in terms of the real masses and the constant widths through

$$\begin{aligned} M_V^2 &= m_V^2 - \mathrm{i}\Gamma_V\, m_V\,, \quad V = W, Z \\ M_H^2 &= m_H^2 - \mathrm{i}\Gamma_H\, m_H\,, \quad M_t = m_t - \mathrm{i}\Gamma_t/2\,, \end{aligned} \tag{8}$$

the corresponding propagators can be written as

$$\begin{aligned} D_{\mathrm{F}}^{\mu\nu}(q) &= \frac{-g^{\mu\nu} + q^\mu q^\nu / M_V^2}{q^2 - M_V^2}\,, \quad D_{\mathrm{F}}(q) = \frac{1}{q^2 - M_H^2}\,, \\ S_{\mathrm{F}}(q) &= \frac{\not{q} + M_t}{q^2 - M_t^2}\,. \end{aligned} \tag{9}$$

In the FWS, the electroweak mixing angle is defined according to

$$\sin^2\theta_{\mathrm{W}} = 1 - \frac{m_W^2}{m_Z^2}\,. \tag{10}$$

It is kept real. For the case of the gauge-invariant CMS, the real gauge boson masses have to be replaced by their complex counterparts and this parameter is therefore complex as well.

Within AMEGIC++ the Yukawa couplings of fermions to the Higgs boson and their kinematical masses are decoupled. This allows us to study, for example, the production of Higgs bosons and their decay into b-quarks, even in those cases where the user prefers to neglect the influence of the b-mass on both the phase-space and the helicity structure.

For the integration over the phase space of the outgoing particles, AMEGIC++ employs an adaptive multichannel method [6]. Similar to their implementation, generic elements for phase-space mappings such as propagator-like structures are provided. The individual Feynman diagrams are analyzed individually and one or more suitable phase-space parametrizations for each diagram are automatically created and stored in library files. As an example, consider Fig. 2, which exhibits a diagram and its translation into propagator and decay parametrizations. These files, both for the amplitudes and the phase-space parametrizations, are compiled and linked to the code before the actual integration starts.

For users of AMEGIC++ only very little intervention is needed. Having specified the process(es), the model framework and its parameters, a first "initialization" run of the code results in the creation of library files. After their compilation, a second, "production" run will generate the results without any further manipulation.

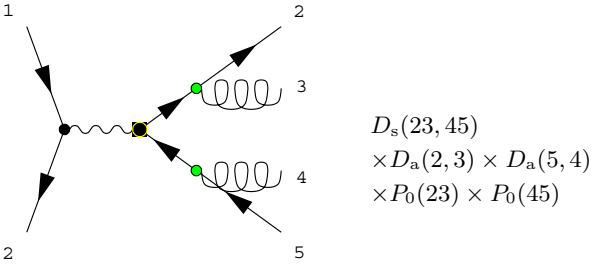

Fig. 2. Translation of a Feynman diagram into a phase-space parametrization. $D_{\mathrm{s,a}}$ denote symmetric or asymmetric decays; the latter ones reproduce the typical feature of collinear emission of particles notorious for gauge theories with massless spin-1 bosons. The propagator terms for massless particles P_0 peak at the minimal allowed invariant mass

4 Numerical results

4.1 Input parameters and phase-space cuts

The SM parameters are given in the G_μ scheme:

$$\begin{aligned} & m_W = 80.419\,\text{GeV}\,, \quad \Gamma_W = 2.12\,\text{GeV}, \\ & m_Z = 91.1882\,\text{GeV}\,, \quad \Gamma_Z = 2.4952\,\text{GeV}, \\ & G_\mu = 1.16639 \times 10^{-5}\,\text{GeV}^{-2}, \\ & \sin^2\theta_\text{W} = 1 - m_W^2/m_Z^2, \\ & \alpha_\text{s} = 0.0925(0.0891) \text{ at } 360(500) \text{ GeV}. \end{aligned} \tag{11}$$

The electromagnetic coupling is derived from the Fermi constant G_μ according to

$$\alpha_\text{em} = \frac{\sqrt{2}\,G_\mu\,M_W^2\,\sin^2\theta_\text{W}}{\pi}. \tag{12}$$

The mass of the Higgs boson is assumed to be $M_H = 130\,\text{GeV}$ and its associated SM tree-level width is $\Gamma_H = 0.00429\,\text{GeV}$. For this Higgs boson mass its branching ratios $H \to b\bar{b}$ and $H \to W^+W^- \to 4f$ are of the same order and therefore both decay channels signify its occurrence as an intermediate state. For the massive fermions, the following masses have been used:

$$\begin{aligned} & m_\mu = 105.6583\,\text{MeV}, \quad m_\tau = 1.777\,\text{GeV}, \\ & m_u = 5\,\text{MeV}, \quad m_d = 10\,\text{MeV}, \\ & m_s = 200\,\text{MeV}, \quad m_c = 1.3\,\text{GeV}, \\ & m_b = 4.8\,\text{GeV}, \\ & m_t = 174.3\,\text{GeV}, \quad \Gamma_t = 1.6\,\text{GeV}. \end{aligned} \tag{13}$$

The constant widths of the electroweak gauge bosons, the Higgs boson and the top quark are introduced via the fixed-width scheme as defined in Sect. 3. CKM mixing of the quark generations and the coupling of the Higgs boson to the very light fermion flavors (e, u, d) is neglected.

Concerning the phase-space integration, the following cuts are applied on the external particles:

$$\begin{aligned} & \theta(l,\text{beam}) > 5^\circ\,, \quad \theta(l,l') > 5^\circ\,, \quad E_l > 10\,\text{GeV}, \\ & \theta(q,\text{beam}) > 5^\circ\,, \quad \theta(l,q) > 5^\circ\,, \quad E_q > 10\,\text{GeV}, \\ & m(q,q') > 10\,\text{GeV}\,, \end{aligned} \tag{14}$$

where $\theta(i,j)$ specifies the angle between the particles i and j in the center-of-mass frame, and l, q and beam denote charged leptons, quarks or gluons and the beam electrons or positrons, respectively. The invariant mass of a jet pair qq' is denoted by $m(q,q')$.

All results presented here are obtained using 10^6 points (before cuts); statistical errors of the Monte Carlo integrations, i.e. one standard deviation, are given in parentheses.

Table 1. The cross sections for possible signals and backgrounds of top quark pair production in $e^+\,e^-$ annihilation. All results in fb for $\sqrt{s} = 360\,\text{GeV}$ (first row) and $\sqrt{s} = 500\,\text{GeV}$ (second row)

Top-quark channels			
Final state	QCD	AMEGIC++ [fb]	HELAC [fb]
$b\bar{b}u\bar{d}d\bar{u}$	yes	32.90(15)	33.05(14)
	yes	49.74(21)	50.20(13)
	no	32.22(34)	32.12(19)
	no	49.42(44)	50.55(26)
$b\bar{b}u\bar{u}gg$	–	11.23(10)	11.136(41)
	–	9.11(13)	8.832(43)
$b\bar{b}gggg$	–	18.82(13)	18.79(11)
	–	24.09(18)	23.80(17)
$b\bar{b}u\bar{d}e^-\bar{\nu}_e$	yes	11.460(36)	11.488(15)
	yes	17.486(66)	17.492(41)
	no	11.312(37)	11.394(18)
	no	17.366(68)	17.353(31)
$b\bar{b}e^+\nu_e e^-\bar{\nu}_e$	–	3.902(31)	3.885(7)
	–	5.954(55)	5.963(11)
$b\bar{b}e^+\nu_e\mu^-\bar{\nu}_\mu$	–	3.847(15)	3.848(7)
	–	5.865(24)	5.868(10)
$b\bar{b}\mu^+\nu_\mu\mu^-\bar{\nu}_\mu$	–	3.808(16)	3.861(19)
	–	5.840(30)	5.839(12)

4.2 Results

First of all, processes have been considered that serve as signals or backgrounds for the production and decay of top pairs, Table 1. Since the branching ratio is practically 100% for the decay of top quarks into bottom quarks and a W ($t \to bW^+$, $\bar{t} \to \bar{b}W^-$), all modes considered include a pair of bottom quarks. In cases involving a mixture of top production and decay and pure QCD diagrams, the relative importance of the different contributions to the total cross section has been estimated by switching on and off the QCD coupling constant. In both cases (the fully hadronic mode $b\bar{b}u\bar{u}d\bar{d}$ and the semileptonic mode $b\bar{b}u\bar{d}e^-\bar{\nu}_e$) the top contribution is by far the dominating channel; the difference of taking into account the QCD contributions or neglecting them is of the order of 2–3%. Also, the total cross section of the fully hadronic channel is substantially larger than the cross section of any other individual $b\bar{b}$+4 jets mode.

For the QCD contributions, a similar pattern arises also in the vector-boson fusion channels, cf. Tables 2 and 3. These channels are characterized by either an electron–positron or an electron–neutrino anti-neutrino pair in the final state, corresponding to either Z boson or to W boson fusion processes, respectively. Again, switching on and off the QCD coupling constant gives rise to differences on the level of a few per cent. In contrast, taking into account the Higgs boson (Table 2) which may be produced in the s-channel through the fusion of two t-channel vector bosons, or neglecting it (Table 3) changes the total cross sections for all channels considered by a factor of 2 or larger. This is

Table 2. The cross sections for different $e^+e^- \to 6f$ final states corresponding to the Higgs production via vector-boson fusion signal. All results in fb for $\sqrt{s} = 360\,\text{GeV}$ (first row) and $\sqrt{s} = 500\,\text{GeV}$ (second row)

Vector fusion with Higgs exchange

Final state	QCD	AMEGIC++ [fb]	HELAC [fb]
$e^-e^+u\bar{u}d\bar{d}$	yes	0.6842(85)	0.6858(31)
	yes	1.237(15)	1.265(5)
	no	0.6453(62)	0.6527(35)
	no	1.206(14)	1.2394(75)
$e^-e^+u\bar{u}e^-e^+$	–	6.06(36)e-03	6.113(87)e-03
	–	6.58(23)e-03	6.614(80)e-03
$e^-e^+u\bar{u}\mu^-\mu^+$	–	9.24(12)e-03	9.04(11)e-03
	–	9.25(17)e-03	9.145(74)e-03
$\nu_e\bar{\nu}_e u\bar{d}d\bar{u}$	yes	1.15(3)	1.176(6)
	yes	2.36(7)	2.432(12)
	no	1.14(3)	1.134(5)
	no	2.35(7)	2.429(13)
$\nu_e\bar{\nu}_e u\bar{d}e^-\bar{\nu}_e$	–	0.426(11)	0.4309(48)
	–	0.916(30)	0.9121(48)
$\nu_e\bar{\nu}_e u\bar{d}\mu^-\bar{\nu}_\mu$	–	0.425(12)	0.4221(30)
	–	0.878(27)	0.8888(47)

Table 3. The backgrounds to Higgs production via vector-boson fusion. All contributions from intermediate Higgs bosons are neglected. Cross sections are given in fb for $\sqrt{s} = 360\,\text{GeV}$ (first row) and $\sqrt{s} = 500\,\text{GeV}$ (second row)

Vector fusion without Higgs exchange

Final state	QCD	AMEGIC++ [fb]	HELAC [fb]
$e^-e^+u\bar{u}d\bar{d}$	yes	0.4838(50)	0.4842(25)
	yes	1.0514(97)	1.0445(51)
	no	0.4502(31)	0.4524(23)
	no	1.0239(79)	1.0227(43)
$e^-e^+u\bar{u}e^-e^+$	–	3.757(98)e-03	3.577(43)e-03
	–	4.082(56)e-03	4.214(46)e-03
$e^-e^+u\bar{u}\mu^-\mu^+$	–	5.201(61)e-03	5.119(70)e-03
	–	5.805(67)e-03	5.828(49)e-03
$\nu_e\bar{\nu}_e u\bar{d}d\bar{u}$	yes	0.15007(53)	0.15070(64)
	yes	0.4755(21)	0.4711(24)
	no	0.12828(42)	0.12793(55)
	no	0.4417(19)	0.4398(21)
$\nu_e\bar{\nu}_e u\bar{d}e^-\bar{\nu}_e$	–	0.04546(13)	0.04564(19)
	–	0.16033(63)	0.16011(78)
$\nu_e\bar{\nu}_e u\bar{d}\mu^-\bar{\nu}_\mu$	–	0.04230(12)	0.04180(16)
	–	0.14383(53)	0.14439(65)

especially pronounced for channels that can be identified as WW-fusion channels with a semileptonic or fully hadronic decay of the W-pair produced by the Higgs decay (i.e. $\nu_e\bar{\nu}_e u\bar{d}e^-\bar{\nu}_e$ and $\nu_e\bar{\nu}_e u\bar{d}\mu^-\bar{\nu}_\mu$, or $\nu_e\bar{\nu}_e u\bar{d}d\bar{u}$, respectively), where the cross sections are larger by one order of magnitude.

Table 4. The cross sections for different $e^+e^- \to 6f$ final states corresponding to the Higgs-strahlung signal. All results given in fb for $\sqrt{s} = 360\,\text{GeV}$ (first row) and $\sqrt{s} = 500\,\text{GeV}$ (second row)

Higgs production through Higgs strahlung

Final state	QCD	AMEGIC++ [fb]	HELAC [fb]
$\mu^-\mu^+\mu^+\nu_\mu e^-\bar{\nu}_e$	–	0.03244(27)	0.03210(15)
	–	0.03747(29)	0.03749(32)
$\mu^-\mu^+u\bar{d}e^-\bar{\nu}_e$	–	0.0924(8)	0.09306(46)
	–	0.1106(22)	0.10901(66)
$\mu^-\mu^+\mu^-\mu^+e^-e^+$	–	2.828(67)e-03	2.923(52)e-03
	–	2.731(65)e-03	2.691(42)e-03
$\mu^-\mu^+u\bar{u}d\bar{d}$	yes	0.2534(24)	0.2540(16)
	yes	0.2634(22)	0.2642(15)
	no	0.2441(23)	0.2471(15)
	no	0.2593(22)	0.2589(14)
$\mu^-\mu^+u\bar{u}u\bar{u}$	yes	1.125(8)e-02	1.135(22)e-02
	yes	8.767(65)e-03	8.978(58)e-03
	no	7.929(57)e-03	8.078(92)e-03
	no	6.098(35)e-03	6.013(26)e-03

Table 5. Background contributions to the Higgs-strahlungs signal for various $6f$ final states. All diagrams with intermediate Higgs bosons have been neglected. Cross sections are given in fb for $\sqrt{s} = 360\,\text{GeV}$ (first row) and $\sqrt{s} = 500\,\text{GeV}$ (second row)

Backgrounds to Higgs strahlung

Final state	QCD	AMEGIC++ [fb]	HELAC [fb]
$\mu^-\mu^+\mu^+\nu_\mu e^-\bar{\nu}_e$	–	0.01845(14)	0.01843(13)
	–	0.03054(23)	0.03092(19)
$\mu^-\mu^+u\bar{d}e^-\bar{\nu}_e$	–	0.05284(57)	0.05209(33)
	–	0.08911(53)	0.08925(48)
$\mu^-\mu^+\mu^-\mu^+e^-e^+$	–	2.204(52)e-03	2.346(49)e-03
	–	2.280(66)e-03	2.277(62)e-03
$\mu^-\mu^+u\bar{u}d\bar{d}$	yes	0.1412(10)	0.1404(11)
	yes	0.2092(12)	0.2075(13)
	no	0.1358(20)	0.1341(12)
	no	0.2040(12)	0.2015(11)
$\mu^-\mu^+u\bar{u}u\bar{u}$	yes	5.937(24)e-03	5.937(25)e-03
	yes	6.134(29)e-03	6.108(27)e-03
	no	2.722(10)e-03	2.710(11)e-03
	no	3.290(12)e-03	3.303(12)e-03

Another mode for Higgs production at an electron–positron collider is Higgs strahlung, where the Higgs boson is radiated off a Z boson in the s-channel. In Table 4, total cross sections for such modes are displayed, where the Z boson decays into muons and the Higgs boson goes into four fermions through a pair of W or Z bosons. In Table 5, identical total cross sections for the same final states, but neglecting the Higgs contribution, are shown. In both cases, again, the size of the pure QCD contributions is found to be small for most final states, i.e. of the order of few per cent. The only exception is for a pair of muons and four identical

Table 6. Cross sections for the process $e^+\,e^- \to \mu^-\mu^+ b\bar{b}b\bar{b}$. All results in fb for $\sqrt{s} = 360\,\text{GeV}$ (first row) and $\sqrt{s} = 500\,\text{GeV}$ (second row)

Multiple Higgs production

Final state	QCD	AMEGIC++ [fb]	HELAC [fb]
$\mu^-\mu^+ b\bar{b}b\bar{b}$	yes	2.560(26)e-02	2.583(26)e-02
	yes	3.096(60)e-02	3.019(43)e-02
	no	1.711(55)e-02	1.666(28)e-02
	no	2.34(12)e-02	2.36(10)e-02

Table 7. Cross sections for $e^+\,e^- \to \mu^-\mu^+ b\bar{b}b\bar{b}$ with all contributions due to intermediate Higgs bosons left out. All results in fb taken for $\sqrt{s} = 360\,\text{GeV}$ (first row) and $\sqrt{s} = 500\,\text{GeV}$ (second row)

Backgrounds to multiple Higgs production

Final state	QCD	AMEGIC++ [fb]	HELAC [fb]
$\mu^-\mu^+ b\bar{b}b\bar{b}$	yes	7.002(32)e-03	7.044(22)e-03
	yes	6.308(24)e-03	6.364(21)e-03
	no	2.955(11)e-03	2.972(12)e-03
	no	3.704(15)e-03	3.695(13)e-03

Table 8. Cross sections for $e^+\,e^- \to \mu^-\mu^+ b\bar{b}b\bar{b}$ with all contributions proportional to the triple Higgs boson coupling left out. All results in fb taken for $\sqrt{s} = 360\,\text{GeV}$ (first row) and $\sqrt{s} = 500\,\text{GeV}$ (second row)

Backgrounds to triple Higgs coupling

Final state	QCD	AMEGIC++ [fb]	HELAC [fb]
$\mu^-\mu^+ b\bar{b}b\bar{b}$	yes	2.512(34)e-02	2.491(31)e-02
	yes	2.578(32)e-02	2.629(53)e-02
	no	1.689(22)e-02	1.702(72)e-02
	no	2.123(27)e-02	2.107(37)e-02

quarks; there, the inclusion of QCD changes the results by roughly 20%, when the Higgs boson is taken into account, and by a factor of roughly two when its contribution is neglected. It is amusing to note that this relative factor of two compares in size with the effect of including the Higgs boson itself. This, however, is true only for the mode that can be imagined as $e^+e^- \to ZH \to ZZZ \to \mu^+\mu^- u\bar{u}u\bar{u}$. In all other cases, as said before, inclusion of QCD has minor effects only; the Higgs boson in contrast roughly doubles the total cross section in all the other channels.

One of the salient research goals at a potential linear collider operating at energies around 500 GeV is the determination of the Higgs potential. For this, the self-couplings of the Higgs bosons have to be checked. In the framework of this publication, results are provided for the channel where the Higgs bosons emerge in Higgs strahlungs-like topologies and decay into a pair of bottom quarks. This leads to final states $\mu^+\mu^- + 4b$, where the muons mainly come from the Z bosons. Results for total cross sections for the process $e^+e^- \to \mu^+\mu^- + 4b$, where contributions mediated by Higgs bosons have been included or completely neglected, are given in Tables 6 and 7, respectively. From the results displayed one can read off that the inclusion of intermediate Higgs bosons enhances the cross sections by a factor of three to four. Again, also the effect of QCD has been checked. For the process involving intermediate Higgs bosons, QCD leads to total cross sections that are larger by roughly 30%–40%, without the Higgs bosons; QCD contributes on the level of factors of two to three. Concerning the influence of the Higgs self-coupling Table 8 shows results for $e^+\,e^- \to \mu^-\mu^+ b\bar{b}b\bar{b}$ with the triple Higgs coupling being neglected but all remaining Higgs boson contributions still taken into account. In comparison with Table 6 no significant contribution of this coupling for a collider energy of 360 GeV can be observed. However, for a center-of-mass energy of 500 GeV the exclusion of the triple Higgs coupling reduces the total cross section by about 10%.

5 Summary of results

In the framework of this comparison, total cross sections for 90 different processes involving six-particle final states have been obtained by the two multi-purpose matrix element generator packages HELAC/PHEGAS and AMEGIC++. The integration over the multidimensional phase space of the final states has been performed with Monte Carlo methods, and in all cases one million MC points have been used. For nearly all cross sections the resulting statistical error was significantly smaller than 1%: roughly 5 per mille. There have been no significant differences between the two codes. To compare the results, for each process i the deviation $s^{(i)}$ of the two resulting cross sections $\sigma_{\text{H}}^{(i)}$ and $\sigma_{\text{A}}^{(i)}$ has been calculated through

$$s^{(i)} = \frac{\sigma_{\text{A}}^{(i)} - \sigma_{\text{H}}^{(i)}}{\sqrt{\left(\Delta\sigma_{\text{A}}^{(i)}\right)^2 + \left(\Delta\sigma_{\text{H}}^{(i)}\right)^2}}\,. \tag{15}$$

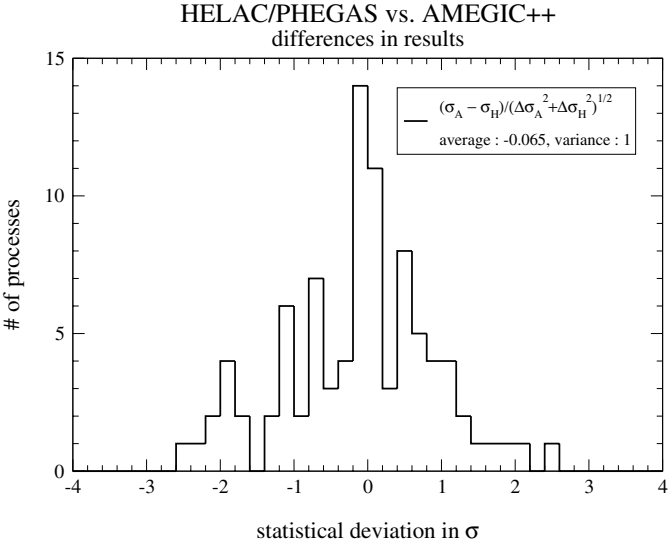

Fig. 3. The distribution of the deviations $s^{(i)}$, given by (15), for the ninety total cross sections i presented in this paper. The average value is $\bar{s} = -0.065$; their variance is $\sigma_s \approx 1$

The distribution of the individual differences is depicted in Fig. 3. The average deviation is $\bar{s} = -0.065$, the variance in their distribution is $\sigma_s \approx 1$. The maximal difference between two cross sections is smaller than three standard deviations, $s^{(\max.)} \approx 2.6$. The distribution of differences follows roughly a Gaussian distribution.

To summarize: Both packages, HELAC/PHEGAS as well as AMEGIC++, lead, with quite different methods, to consistent results for total cross sections for a large number of different processes with six particles in the final state. This provides an independent check of the precision level of the two codes, which can be considered as successfully tested.

Acknowledgements. The authors thank the Center for High Performance Computing Dresden (ZHR) for providing their resources and BMBF for financial support. The work of FK was supported by the EC 5th Framework Programme under contract number HPMF-CT-2002-01663. CGP also acknowledges support from the EC project "Multi-particle Processes and Higher Order Corrections", HPMF-CT-2002-01622. S.S. wants to thank GSI Darmstadt for financial support.

References

1. A. Kanaki, C.G. Papadopoulos, Comput. Phys. Commun. **132**, 306 (2000) [hep-ph/0002082]
2. C.G. Papadopoulos, Comput. Phys. Commun. **137**, 247 (2001) [hep-ph/0007335]
3. F. Krauss, R. Kuhn, G. Soff, JHEP **0202**, 044 (2002) [hep-ph/0109036]
4. S. Dittmaier, M. Roth, Nucl. Phys. B **642**, 307 (2002) [hep-ph/0206070]
5. K. Kolodziej, hep-ph/0210199
6. F.A. Berends, R. Pittau, R. Kleiss, Nucl. Phys. B **424**, 308 (1994) [hep-ph/9404313]; R. Kleiss, R. Pittau, Comput. Phys. Commun. **83**, 141 (1994) [hep-ph/9405257]
7. F. Gangemi, G. Montagna, M. Moretti, O. Nicrosini, F. Piccinini, Eur. Phys. J. C **9**, 31 (1999) [hep-ph/9811437]; F. Gangemi, G. Montagna, M. Moretti, O. Nicrosini, F. Piccinini, Nucl. Phys. B **559**, 3 (1999) [hep-ph/9905271]; F. Gangemi, hep-ph/0002142
8. M. Moretti, T. Ohl, J. Reuter, hep-ph/0102195
9. W. Kilian, LC-TOOL-2001-039
10. T. Stelzer, W.F. Long, Comput. Phys. Commun. **81**, 357 (1994) [hep-ph/9401258]
11. F. Maltoni, T. Stelzer, JHEP **0302**, 027 (2003) [hep-ph/0208156]
12. F. Caravaglios, M. Moretti, Phys. Lett. B **358**, 332 (1995) [hep-ph/9507237]; Z. Phys. C **74**, 291 (1997) [hep-ph/9604316]
13. T. Ohl, Comput. Phys. Commun. **120**, 13 (1999) [hep-ph/9806432]
14. H. Murayama, I. Watanabe, K. Hagiwara, KEK-91-11
15. M.W. Grunewald et al., hep-ph/0005309
16. J.A. Aguilar-Saavedra et al. [The ECFA/DESY LC Physics Working Group], hep-ph/0106315
17. S. Dittmaier, hep-ph/0308079
18. M.L. Mangano, S.J. Parke, Phys. Rep. **200**, 301 (1991), and references therein [hep-ph/9212246]
19. W.T. Giele, Properties and calculations of multiparton processes, Ph.D. thesis (University of Leiden 1989)
20. P.D. Draggiotis, R.H.P. Kleiss, C.G. Papadopoulos, Phys. Lett. B **439**, 157 (1998) [hep-ph/9807207]; Eur. Phys. J. C **24**, 447 (2002) [hep-ph/0202201]
21. F. Caravaglios, M.L. Mangano, M. Moretti, R. Pittau, Nucl. Phys. B **539**, 215 (1999) [hep-ph/9807570]; M.L. Mangano, M. Moretti, F. Piccinini, R. Pittau, A.D. Polosa, JHEP **0307**, 001 (2003) [hep-ph/0206293]
22. J.G.M. Kuijf, Multiparton production at hadron colliders, Ph.D. thesis (University of Leiden 1991)
23. HELAC-PHEGAS: automatic computation of helicity amplitudes and cross sections, A. Kanaki, C.G. Papadopoulos, Second CPP Symposium-Computational Particle Physics, KEK Proceedings 2002-11, edited by Y. Kurihara, August 2002, pp. 20–25
24. Andre van Hameren, C.G. Papadopoulos, talk given by A. v. Hameren at the 4th ECFA/DESY workshop on Physics and Detectors for a Linear Electron-Positron collider, NIKHEF, Amsterdam, The Netherlands, April 2003
25. See e.g. G. Lopez Castro, J.L. Lucio, J. Pestieau, Mod. Phys. Lett. A **6**, 3679 (1991); M. Nowakowski, A. Pilaftsis, Z. Phys. C **60**, 121 (1993) [hep-ph/9305321]; E.N. Argyres et al., Phys. Lett. B **358**, 339 (1995) [hep-ph/9507216]; W. Beenakker et al., Nucl. Phys. B **500**, 255 (1997) [hep-ph/9612260], and references therein
26. A. Denner, S. Dittmaier, M. Roth, D. Wackeroth, Nucl. Phys. B **560**, 33 (1999) [hep-ph/9904472]
27. T. Gleisberg, F. Krauss, K.T. Matchev, A. Schälicke, S. Schumann, G. Soff, JHEP **0309**, 001 (2003) [hep-ph/0306182]
28. T. Gleisberg, S. Höche, F. Krauss, A. Schälicke, S. Schumann, J. Winter, CERN–TH/2003-284 and hep-ph/0311263
29. R. Kuhn, F. Krauss, B. Ivanyi, G. Soff, Comput. Phys. Commun. **134**, 223 (2001) [hep-ph/0004270]
30. S. Catani, F. Krauss, R. Kuhn, B.R. Webber, JHEP **0111**, 063 (2001) [hep-ph/0109231]; F. Krauss, JHEP **0208**, 015 (2002) [hep-ph/0205283]
31. R. Kleiss, W.J. Stirling, Nucl. Phys. B **262**, 235 (1985); A. Ballestrero, E. Maina, S. Moretti, Nucl. Phys. B **415**, 265 (1994)
32. A. Denner, H. Eck, O. Hahn, J. Kublbeck, Nucl. Phys. B **387**, 467 (1992)